

Effects of the Two-Gap Nature on the Microwave Conductivity of 39 K Polycrystalline MgB₂ Films

Sang Young Lee^{1,*}, J. H. Lee¹, Jung Hoon Han^{2,3}, S. H. Moon⁴, H. N. Lee⁵, James C. Booth⁶ and J. H. Claassen⁷

1 Department of Physics and Center for Optoelectronic and Microwave Devices, Konkuk University, Seoul 143-701, Korea

2 Department of Physics, Sungkyunkwan University, Suwon, Korea,

3 CSCMR, Seoul National University, Seoul 151-747, Korea

4 School of Materials Science, Seoul National University, Seoul, Korea

5 LG Electronic Institute of Technology, Seoul, Korea

6 National Institute of Standards and Technology, Boulder, CO, U.S.A.

7 Naval Research Laboratory, Washington D.C., U.S.A.

The surface resistance (R_S) and the real part (σ_1) of the microwave complex conductivity of a ~ 380 nm-thick polycrystalline MgB₂ film with the critical temperature (T_C) of 39.3 K were investigated at ~ 8.5 GHz as a function of temperature. Two coherence peaks were observed in the σ_1 versus temperature curve at temperatures of $\sim 0.5 T_C$ and $\sim 0.9 T_C$, respectively, providing a direct evidence for the two-gap nature of MgB₂. The film appeared to have a π -band gap energy of 1.8 meV. For the MgB₂ film ion-milled down to the thickness of ~ 320 nm, two coherence peaks were still observed with the first conductivity peak at $\sim 0.6 T_C$. Reduction of T_C by 3 K and reduced normal-state conductivity at T_C were observed along with an enhanced π -band gap energy of 2.1 meV and a reduced R_S at temperatures below 15 K for the ion-milled film. Calculations based on the gap energies from the weak coupling Bardeen-Cooper-Schrieffer theory and the strong coupling theory suggest that both the σ -band and the π -band contribute to σ_1 of the polycrystalline MgB₂ films significantly. Our results are in contrast with the observation of single coherence peak at $\sim 0.6 T_C$ and dominant role of the π -band in the microwave conductivity of c -axis oriented MgB₂ films as reported by Jin *et al.* [Phys. Rev. Lett. 91, 127006 (2003)]. Variations in the inter-band coupling constants with the level of disorder can account for the different T_C and σ_1 behavior for the as-grown and ion-milled films.

Our results suggest that enhanced inter-band scattering can improve microwave properties of MgB₂ films at low temperatures due to the larger π -band gap despite the reduction of T_C .

PACS Numbers: 74.25.Fy, 74.25.Nf, 74.70.Ad

I. Introduction

Since the discovery of superconductivity in magnesium diboride (MgB₂)¹, MgB₂ has been known as the first superconductor material with two energy gaps, one in the two-dimensional σ -band and the other in the three dimensional π -band with very small inter-band scattering between them^{2,4}. Accordingly, MgB₂ has shown unique properties that have been unheralded from any superconductors with a single gap⁵. Richness in the observed unique properties of MgB₂ may also originate from the relative weight with which each band contributes to the measured physical properties. For instance, both bands are known to play an important role in determining the specific heat of MgB₂^{6,7}, and explaining anomalous temperature-dependent anisotropy of the upper critical field^{8,9}. Meanwhile Kim *et al.*

reported that the measured penetration depth (λ) of MgB₂ is mainly due to the role of the σ -band¹⁰.

Recently, other interesting results have been reported with regard to the microwave conductivity of MgB₂ by Jin *et al.*¹¹. They measured the microwave conductivity of MgB₂ and reported that contribution of the σ -band is insignificant with regard to the real part of the complex microwave conductivity of MgB₂ films. According to them, observations of single coherence peak at $T/T_C \sim 0.6$ and non-existence of any coherence peak near T_C support their arguments, with the peak at $T/T_C \sim 0.6$ attributed to the π -band. Jin *et al.*'s results, however, appear inconsistent with those by Kim *et al.*⁹, who reported that the measured penetration depth, whose magnitude is directly related with the imaginary part of the microwave complex conductivity, is mostly due to the σ -band. The fact that the films used by both Jin *et al.* and Kim *et al.*

were prepared by the same researchers using the same growth technique makes this kind of inconsistency with regard to the microwave conductivity of MgB₂ much more puzzling.

Here we study the surface resistance R_S and the microwave conductivity of high-quality polycrystalline MgB₂ films as a function of the temperature. The R_S is measured by a TE₀₁₁ mode dielectric resonator method, the same kind of measurement method used by Jin *et al.*¹¹ with λ measured by the mutual inductance measurement method proposed by Claassen *et al.*¹². This gives the absolute value of λ independent of the microwave measurements, in contrast to the analysis of Jin *et al.* [Ref. 11] which infers λ from a fit of the microwave data to a specific model. The R_S of an as-grown MgB₂ film is compared with that of the same film with reduced thickness after the ion-milling. A crossover in the temperature dependence of the R_S is observed between the two films as has previously been reported for the two kinds of MgB₂ films which were separately prepared¹³. Two prominent peaks are observed from both films with each peak attributable to the role of the two bands in the conductivity of MgB₂, which is in contrast with that reported by Jin *et al.*¹¹. We argue that R_S and the microwave conductivity of the films can be understood in the context of the two-gap scenario.

II. Experimental

A MgB₂ film (MgB₂-21A) with the T_C of ~ 39 K was prepared on 0.5 mm-thick *c*-cut sapphire by the two-step process where boron films deposited on the substrates are annealed in a Mg vapor environment inside quartz tubes. The dimensions of the MgB₂ film are 14 x 14 mm², with the thickness of ~ 380 nm. More details of the sample preparation have been reported elsewhere¹⁴. The film appeared to be single phase from the X-ray diffraction (XRD) data. Typical dc resistance data also showed that the films had the critical onset temperature of ~ 39 K and the transition width less than ~ 0.3 K.

The effective surface resistance R_S^{eff} of MgB₂-21A was measured at temperatures between 6.5 K and 45 K at ~ 8.5 GHz using a TE₀₁₁ mode cavity resonator made of oxygen-free high conductivity copper (OFHC) loaded with a rutile-phase TiO₂ (henceforth called ‘rutile’) rod having the dimensions of 3.88 mm in diameter and 2.73 mm in height. The diameter of the OFHC cavity is 9 mm. During measurements, an epitaxially-grown YBCO film, which was used as a reference, was placed at the bottom of the cavity with the MgB₂ film placed at the top. We note that the electric field for the TE₀₁₁ mode is parallel to the surface of each film used as the endplates of the cavity in its direction and has a rotational symmetry around the axis perpendicular to the film

surface. The R_S of the YBCO film and the loss tangent of the rutile rod were separately measured to get the R_S of the MgB₂ film from the unloaded Q of the rutile-loaded resonator with the MgB₂ film at the top and the YBCO film at the bottom. Details for this measurement process have been published elsewhere¹⁵. The temperature was stable within ± 0.15 K. The R_S^{eff} obtained from the measured unloaded Q was reproducible within 5 % with errors in R_S^{eff} at 8.5 GHz up to ± 15 % below 10 K due to errors in the measured loss tangent of rutile.

The intrinsic surface resistance R_S was calculated using the equation for the effective surface impedance Z_S^{eff} . A rigorous TE₀₁₁ mode analysis was performed with the cutoff frequency in the substrate region considered, and the relation between Z_S^{eff} and the intrinsic surface impedance Z_S is expressed by

$$Z_S^{eff} = G_S Z_S = \frac{\coth(\beta_{z3} t) - (\beta_h / \beta_{z3})}{1 - (\beta_h / \beta_{z3}) \coth(\beta_{z3} t)} \times \frac{i\omega\mu_0}{\beta_{z3}} \quad (1)$$

Here $Z_S = i\omega\mu_0/\beta_{z3}$ and $\beta_{z3}^2 = i\omega\mu_0\sigma^*$ with $\sigma^* (= \sigma_1 - i\sigma_2)$ denoting the microwave complex conductivity, ω , the angular frequency, and $\beta_h = -\beta_{z4} \cot(\beta_{z4} l)$ with β_{z4} denoting the complex propagation constant in the substrate region, t , the film thickness and l , the substrate thickness¹⁶. β_h could be obtained with the measured surface resistance of the OFHC plate at the back of the substrate taken into account. For reference, $\beta_h = (-2.07 \times 10^3 - 4.07 \times 10^{-1} i)/m$ with $\beta_{z4} = (2.26 \times 10^{-5} - 6.55 \times 10^2 i)$ at ~ 10 K for MgB₂-21A, which changes just a little at different temperatures with the values of $\beta_h = (-2.07 \times 10^3 - 4.32 \times 10^{-1} i)/m$ and $\beta_{z4} = (2.28 \times 10^{-5} - 6.53 \times 10^2 i)$ at ~ 38 K. Since $\beta_{z3} = (\omega\mu_0/4)^{1/2} f_1(\sigma_1, \sigma_2)$ and $Z_S = (\omega\mu_0/4)^{1/2} f_2(\sigma_1, \sigma_2)$ with

$$f_1 = [\{(p+\sigma_1)^{1/2} + (p-\sigma_1)^{1/2}\} - i\{(p-\sigma_1)^{1/2} - (p+\sigma_1)^{1/2}\}]/p,$$

$$f_2 = [\{(p+\sigma_1)^{1/2} - (p-\sigma_1)^{1/2}\} + i\{(p-\sigma_1)^{1/2} + (p+\sigma_1)^{1/2}\}]/p \quad (2)$$

and $p = (\sigma_1^2 + \sigma_2^2)^{1/2}$ ¹⁷, we took the σ^* values that give best fit to the measured R_S^{eff} (i.e., the real part of Z_S^{eff}) and λ (i.e., the real part of β_{z3}) and obtained the intrinsic surface resistance R_S from $R_S = \text{Re}\{(i\mu_0\omega/\sigma^*)^{1/2}\}$. We note that the σ^* values obtained here are almost the same as those from the impedance transformation method¹⁸. The normal-state intrinsic surface resistance R_{SN} is also calculated from the measured normal-state effective values (R_{SN}^{eff}) with the finite thickness of the films taken into account and assuming normal skin effect (i.e., $R_{SN} = X_{SN}$ with X_{SN} denoting the normal-state surface reactance)

for MgB_2 in the normal state. The normal-state conductivity (resistivity) is $1.26 \times 10^7/\Omega\text{-m}$ ($7.94 \mu\Omega\text{-cm}$) at T_C .

Later the as-grown MgB_2 -21A film was ion-milled and designated MgB_2 -21I, and then re-measured. In preparing the ion-milled film, the surface of the MgB_2 film was etched by argon ion-milling under an angle of 70 degree with respect to the film plane. The etching rate was ~ 10 nm/min with a beam voltage of 500 V and a current density of 0.28 mA/cm^2 . MgB_2 -21I has the T_C of 36.3 K with the thickness ~ 320 nm. The normal-state conductivity (resistivity) is $6.20 \times 10^6/\Omega\text{-m}$ ($16.1 \mu\Omega\text{-cm}$) at T_C for MgB_2 -21I.

III. Results and Discussion

Figure 1(a) shows the temperature dependence of R_S^{eff} of MgB_2 -21A and 21I measured at 8.5 GHz. It is seen that the R_S^{eff} values of both films are lower than $\sim 10 \mu\Omega$ at 7 K, a value comparable to the surface resistance of high-quality MgB_2 films including c -axis oriented films¹⁹⁻²¹. This shows that the surface resistance of our film is affected little by their polycrystalline nature at low temperatures. In the figure we see that the surface resistance of MgB_2 -21I appears different from that of MgB_2 -21A with increase of $\sim 290 \text{ m}\Omega$ in R_{SN}^{eff} and decrease of $\sim 3 \text{ K}$ in T_C with T_C of 36.3 K for MgB_2 -21I. A crossover in the R_S^{eff} vs. T data is also seen between 21A and 21I in the figure, with the R_S^{eff} of 21I appearing lower than that of 21A at temperatures below $\sim 13 \text{ K}$. Similar changes in the R_S^{eff} values have repeatedly been observed for high-quality MgB_2 films after the ion-milling, which could be explained within the scenario of the two-gap model with the changes in crossover attributed to the enhanced inter-band scattering between the σ -band and the π -band¹³. λ was also measured as a function of temperature for both MgB_2 films, as shown in the inset of Fig. 1(a). In the inset, we see that the λ value at 0 K (λ_0) are $\sim 90 \text{ nm}$ for MgB_2 -21A and $\sim 100 \text{ nm}$ for MgB_2 -21I, respectively, which are comparable to the value for c -axis oriented MgB_2 films reported by other researchers¹¹.

We obtained the intrinsic surface resistance R_S of the two MgB_2 films from the measured R_S^{eff} and λ values, which are displayed in Fig. 1(b). Here we also see that the surface resistance of MgB_2 -21I becomes different from that of MgB_2 -21A with increase of $\sim 20 \text{ m}\Omega$ in R_{SN} and decrease of $\sim 3 \text{ K}$ in T_C due to the ion-milling. A crossover in the R_S vs. T data is also seen between 21A and 21I in the figure, with the R_S of 21I appearing lower than that of 21A at temperatures below $\sim 15 \text{ K}$. The R_S of both films showed exponential temperature dependence at low temperatures as displayed in Fig. 1(c), which reflects the s -wave nature of the order parameter in

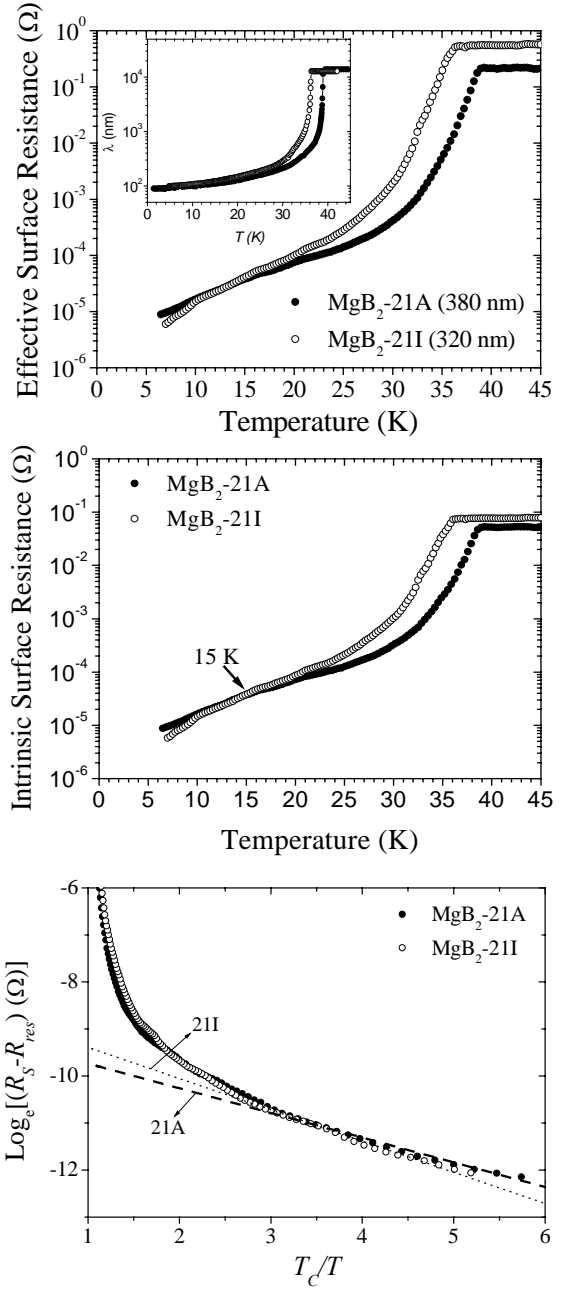


Fig. 1. (a) The effective surface resistance R_S^{eff} of the as-grown MgB_2 film MgB_2 -21A and the ion-milled MgB_2 film MgB_2 -21I. Reduced T_C and Enhanced R_{SN}^{eff} are seen after the ion-milling. A crossover in the R_S^{eff} vs. T data is seen at the temperature of $\sim 13 \text{ K}$ between MgB_2 -21A and MgB_2 -21I. Inset: The temperature dependence of the penetration depth for MgB_2 -21A and MgB_2 -21I. (b) The intrinsic surface resistance R_S of the as-grown MgB_2 film MgB_2 -21A and the ion-milled MgB_2 film MgB_2 -21I calculated from the measured R_S^{eff} and the penetration depth with the film thickness taken into account. (c) $\ln(R_S - R_{\text{res}})$ vs. T_C/T curves for MgB_2 -21A and MgB_2 -21I. The dashed (dotted) line represents an exponential behavior with the slope characterized by $\Delta(0)/k_B T_C = 0.52$ (0.66) for MgB_2 -21A (MgB_2 -21I). The extrapolated R_{res} is $4 \times 10^{-6} \mu\Omega$ for MgB_2 -21A, and R_{res} is not subtracted at all for MgB_2 -21I.

the π -band considering that the π -band would be mostly responsible for the microwave loss due to quasi-particle excitations at low temperatures. The π -band gap energies could be obtained from the R_S values of the films at low temperatures, which are ~ 1.8 meV and ~ 2.1 meV for MgB₂-21A and MgB₂-21I, respectively.

The measured R_S^{eff} and λ also enable us to get the values for the conductivity σ_l of the MgB₂ films, which could be used for investigating effects of its gap energy values on σ_l . We show the temperature dependence of σ_l for the as-grown and the ion-milled MgB₂ films in Fig. 2.

We also see two peaks for both films with prominent peaks at ~ 21 K ($T/T_C \sim 0.53$) and ~ 36 - 37 K ($T/T_C \sim 0.9$) for 21A and the peaks at ~ 22 K ($T/T_C \sim 0.61$) and ~ 33 K ($T/T_C \sim 0.9$) for 21I. It seems that the two peaks provide a signature for the existence of two energy gaps in MgB₂, with the peaks at $T/T_C \sim 0.5 - 0.6$ due to the gap in the π -band and the other peaks at $T/T_C \sim 0.9$ due to the gap in the σ -band. This is, however, in contrast with what has been reported by Jin *et al.*, who observed only one peak at $T/T_C \sim 0.6$ in the σ_l vs. T data and attributed the coherence peak to the π -band¹¹. They reported that lack of the coherence peak at the temperature near T_C is due to insignificant contribution of the σ -band to the real part σ_l . We could also observe two conductivity peaks for the ion-milled film 21I, with the temperature dependence of σ_l appearing somewhat different from that for the as-grown film 21A. We note in Fig. 2 that the peak at ~ 21 K appears somewhat suppressed compared to the peak near T_C after the ion-milling.

Another interesting thing to note in the figure is the existence of a crossover between the data for 21A and 21I, which shows that existence of the crossover in the R_S vs. T curves for the two MgB₂ films is indeed related with their microwave conductivity data with the σ_l values of 21I becoming smaller than those of 21A at ~ 25 K.

To better understand the role of each band in determining the conductivity of the MgB₂ films, we provide a theoretical explanation for the conductivity data using the following relation.

$$\sigma_l / \sigma_{ln} = A_\sigma \sigma_{l\sigma} / \sigma_{n\sigma} + B_\pi \sigma_{l\pi} / \sigma_{n\pi}. \quad (3)$$

Here σ_{ln} denote the total microwave conductivity in the normal state, with $\sigma_{l\sigma}$ ($\sigma_{l\pi}$) and $\sigma_{n\sigma}$ ($\sigma_{n\pi}$) for the microwave conductivity in the superconducting and normal state due to the σ -band (π -band), respectively. A_σ and B_π denote the relative weighting factors with $A_\sigma + B_\pi = 1$, which determines the relative contribution of each band to the microwave conductivity. In Eq. (3), contribution of inter-band scattering to the conductivity is not considered, with the total conductivity of MgB₂ films

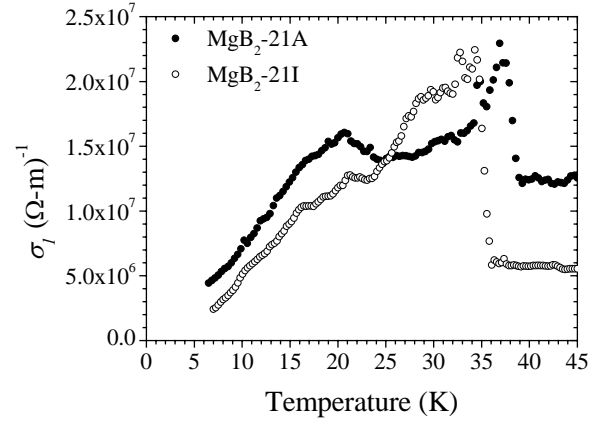


Fig. 2. The temperature dependence of σ_l for MgB₂-21A and MgB₂-21I. Two peaks are shown in the σ_l vs. T data at $T/T_C \sim 0.53$ and ~ 0.9 for MgB₂-21A and at $T/T_C \sim 0.6$ and ~ 0.9 for MgB₂-21I. The peak at $T/T_C \sim 0.6$ for MgB₂-21I appears less pronounced compared to that at $T/T_C \sim 0.53$ for MgB₂-21A.

simply given by the sum of the microwave conductivity of each band. From the values of the $\sigma_{ln}(T_C) = 1.26 \times 10^7 / \Omega\text{-m}$ for MgB₂-21A and $6.20 \times 10^6 / \Omega\text{-m}$ for MgB₂-21I, and the relation of $\sigma_{ln}(T_C) \sim \epsilon_0 \hbar \omega_p^2 / \Gamma$ with $\hbar \omega_p = 5.9$ eV for the plasma frequency which is assumed equal in the two bands²², we get $\Gamma \sim 37$ meV and $\Gamma \sim 75$ meV for the scattering rate in MgB₂-21A and MgB₂-21I, respectively. Since our MgB₂ film is regarded as dirty superconductors with the scattering rate much larger than the gap energy of ~ 7 meV for the σ -band, we used Mattis-Bardeen theory with $\sigma_{l,i} / \sigma_{ni}$ expressed by²³

$$\frac{\sigma_{l,i}(\omega)}{\sigma_{n,i}(\omega)} = \frac{1}{2\omega} \int_{-\infty}^{\infty} d\Omega \left[\tanh \frac{\hbar(\Omega + \omega)}{2k_B T} - \tanh \frac{\hbar\Omega}{2k_B T} \right] \times [N_i(\Omega)N_i(\Omega + \omega) + M_i(\Omega)M_i(\Omega + \omega)] \quad (4)$$

where

$$N_i(\Omega) = \text{Re} \left\{ \frac{|\hbar\Omega|}{\sqrt{(\hbar\Omega)^2 - \Delta_i^2}} \right\},$$

$$M_i(\Omega) = \text{Re} \left\{ \frac{\Delta_i \text{sgn}(\Omega)}{\sqrt{(\hbar\Omega)^2 - \Delta_i^2}} \right\}, \quad (5)$$

with ω denoting the measured angular frequency, Δ_i , the gap energy in the σ -band (π -band) for $i = 1$ (2), k_B , the Boltzmann constant, T , the temperature. A BCS-like multiple-gap model proposed by Liu *et al.* was used to obtain the gap energies corresponding to the σ -band and the π -band, which is given by

$$\Delta_i = \sum_j \lambda_{ij} \Delta_j \int_0^{\hbar\omega_C} dE \frac{\tanh \sqrt{E^2 + \Delta_j^2}}{\sqrt{E^2 + \Delta_j^2}}. \quad (6)$$

Here Δ_i is the same as defined in Eq. (4), λ_{ij} , the electron-phonon coupling constant due to scattering of an electron from band i to band j , $\hbar\omega_C$, the cutoff energy which is assumed equal in both bands. We used the values of $\lambda_{11} = 0.96$, $\lambda_{12} = 0.19$, $\lambda_{21} = 0.14$, $\lambda_{22} = 0.23$ with $\hbar\omega_C = 7.5$ meV for MgB₂-21A having the T_C of 39.3 K and the π -band gap energy $\Delta_\pi(0)$ of 1.8 meV, where the value for λ_{11} is a little smaller than the corresponding value of $\lambda_{11} = 0.98$ for 40 K MgB₂ as given in Ref. 2 with the lower T_C taken into account^{24, 25}. In this case, the calculated gap energy values from Eq. (6) with $\hbar\omega_C = 7.5$ meV become comparable with those by *ab-initio* calculations employing the strong-coupling theory. We note that we used the relation of $\lambda_{ij} = V_{ij}N_j$ in obtaining the λ_{ij} values, where V_{ij} denotes the 2 x 2 effective phonon-mediated electron-electron interaction matrix, N_1 (N_2), the partial density of states of the σ -band (π -band) with $N_1 / N_2 = 1.35$ as given in Ref. 2. For reference, the coupling constants used for MgB₂-21A correspond to $V_{12}/V_{11} \approx 0.15$. We also note that the difference between the value of $\hbar\omega_C = 7.5$ meV and the physically relevant logarithmically averaged phonon energy $\hbar\omega_{ln} = 56.2$ meV could be removed if strong-coupling corrections are considered².

In Fig. 3(a), we compare the measured σ_l/σ_n values with those calculated for different values of A_σ and B_π . In the figure, the measured conductivity appears to agree well with the calculated values for $A_\sigma = 0.6$ and $B_\pi = 0.4$ at temperatures below ~ 20 K, showing significant contribution of the σ -band to the conductivity.

Figure 3(b) shows the gap energies calculated from Eq. (6) using the coupling constants for MgB₂-21A, which are compared with those from the strong coupling theory³. In the figure, we see that the difference between the two sets of values becomes larger as the temperature gets closer to T_C , with the gap energy from the strong-coupling theory larger than that from Eq. (6) by ~ 0.5 meV for the σ -band and ~ 0.15 meV for the π -band at 38 K. However, the values of $A_\sigma = 0.6$ and $B_\pi = 0.4$ still give the best fit to the measured results even if the gap energies from the strong coupling theory are used. For instance, in Fig. 3(c), we see no significant difference in the overall shapes of the σ_l/σ_n curve due to the σ -band ($\sigma_{1\sigma}/\sigma_{n\sigma}$) and that due to the π -band ($\sigma_{1\pi}/\sigma_{n\pi}$), with the peak position in the $\sigma_{1\sigma}/\sigma_{n\sigma}$ and the $\sigma_{1\pi}/\sigma_{n\pi}$ data remaining the same regardless of the theory used for the two gap energies.

In Fig. 4(a), the experimental conductivity values of

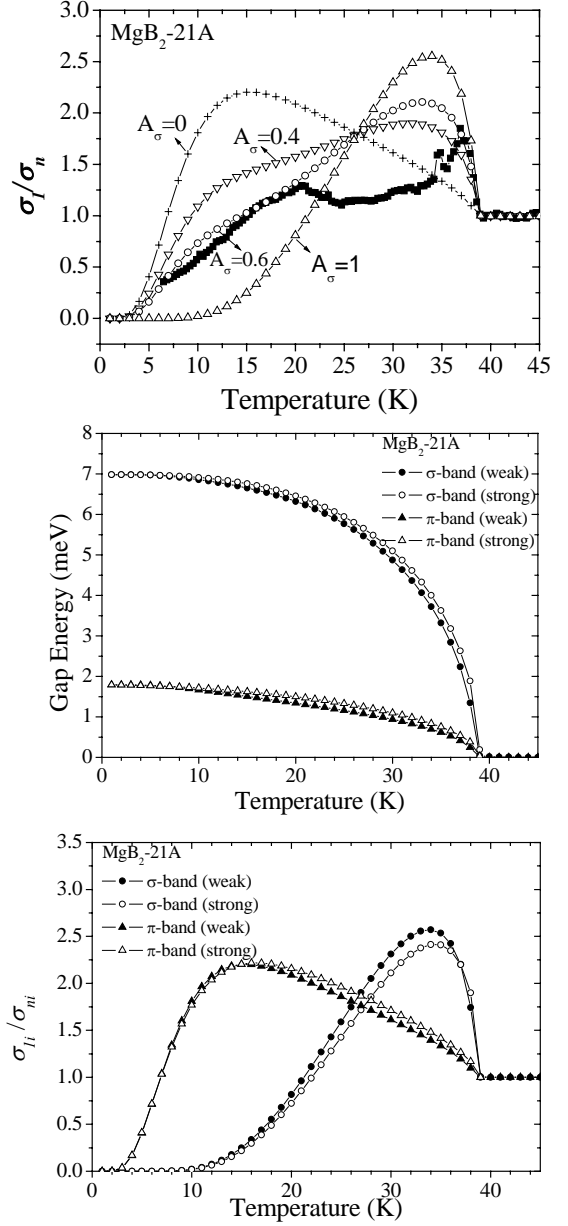


Fig. 3. (a) The measured temperature dependence of σ_l/σ_n for MgB₂-21A compared with the calculated σ_l/σ_n for different values of A_σ and B_π in Eq. (3). The best fitted results are seen for $A_\sigma = 0.6$ and $B_\pi = 0.4$ at temperatures below ~ 20 K. (b) A comparison between the calculated gap energy values using Eq. (6) (filled symbols) and those using the strong-coupling theory (open symbols) for the σ -band and the π -band of MgB₂-21A. The difference becomes larger as the temperature gets closer to T_C , with the gap energy from the strong-coupling theory larger than that from Eq. (6) by ~ 0.5 meV and ~ 0.15 meV at 38 K. (c) The temperature dependence of the normalized σ_l for the σ -band ($i = 1$, circle) and the π -band ($i = 2$, triangle) calculated using the gap energy values from Eq. (6) and those from the strong-coupling theory. Changes in the peak position of the curves for the σ -band and the π -band appear not significant despite differences in the gap energy values calculated using Eq. (6) and the strong-coupling theory, respectively.

MgB₂-21I are compared with those calculated using different values of A_σ and B_π . We used coupling constants of $\lambda_{11} = 0.87$, $\lambda_{12} = 0.245$, $\lambda_{21} = 0.18$, $\lambda_{22} = 0.23$ in calculating the gap energies of MgB₂-21I having T_C of 36.3 K and $\Delta_\pi(0)$ of 2.1 meV. In using the coupling constants for MgB₂-21I, we considered the following things. At first, to consider the reduction of the T_C , which is directly affected by the gap energy in the σ -band, we used smaller intra-band pairing interaction V_{11} in the σ -band for MgB₂-21I than that for MgB₂-21A. Accordingly the intra-band pairing interaction V_{22} in the π -band for MgB₂-21I would be no larger than that for MgB₂-21A, and we used the same value for MgB₂-21A. Finally, to consider the enhanced $\Delta_\pi(0)$ for MgB₂-21I, we used larger inter-band pairing interaction V_{12} ($= V_{21}$) for MgB₂-21I than that for MgB₂-21A. We could also use smaller V_{22} for MgB₂-21I to take the reduced V_{11} into consideration. In this case, however, V_{12} for MgB₂-21I should be even larger than the values used here to match the calculated T_C with the measured T_C , which doesn't make any significant difference with regard to explaining the reduced T_C . For reference, the coupling constants used for MgB₂-21I correspond to $V_{12}/V_{11} = 0.21$.

We note that there have been reports on the effects of inter-band scattering on the energy gaps; Brinkman *et al.* predicted collapse of the two gaps into one gap for MgB₂ having increased inter-band scattering due to impurities²⁶ and Yates *et al.* observed correlation between T_C and the electron-phonon coupling constant by studying Raman-active E_{2g} mode of a MgB₂ film as a function of thickness through a thin film²⁷. In Fig. 4(a), the measured σ_1/σ_n values appear to agree well with those calculated with $A_\sigma = 0.4$ and $B_\pi = 0.6$ at temperatures below ~ 25 K, which also suggest significant contribution of the σ -band to the microwave conductivity of polycrystalline MgB₂ films. As mentioned earlier, for the ion-milled sample 21I, the peak at ~ 22 K appear much suppressed compared to that at 33-34 K, which is different from what we observed for the as-grown sample 21A. We note that the values of $A_\sigma = 0.4$ and $B_\pi = 0.6$ change little even if the gap energies from the strong coupling theory were used. The gap energy values from the weak coupling theory are compared with those by the strong coupling theory in the inset of Fig. 4(a), where the gap energy from the strong coupling theory also gets larger than that from the weak coupling theory at temperatures closer to T_C .

We compare σ_1/σ_n vs. T/T_C data for 21I with those for 21A in Fig. 4(b). One thing we note in the figure is the shift in the peak position related with the π -band from $T/T_C = 0.53$ for 21A to $T/T_C = 0.61$ for 21I after the ion-milling, which could be attributed to the increased inter-band scattering rate, i.e., the increased inter-band coupling constants for 21I as seen in the inset of Fig. 4(b).

In the inset, the peak position of $T/T_C \sim 0.46$ in the calculated $\sigma_{1\pi}/\sigma_{n\pi}$ for the π -band of MgB₂-21A (labeled 'A') appears shifted to $T/T_C \sim 0.55$ for MgB₂-21I (labeled 'I'), which is in qualitative agreements with the change in the peak position due to the π -band as seen in Fig. 4(a). Meanwhile, we also see in the inset that the peak position of $T/T_C \sim 0.87$ in the calculated $\sigma_{1\sigma}/\sigma_{n\sigma}$ for the σ -band remains almost the same for MgB₂-21A and MgB₂-21I despite changes in the coupling constants.

The difference in the microwave conductivity and T_C

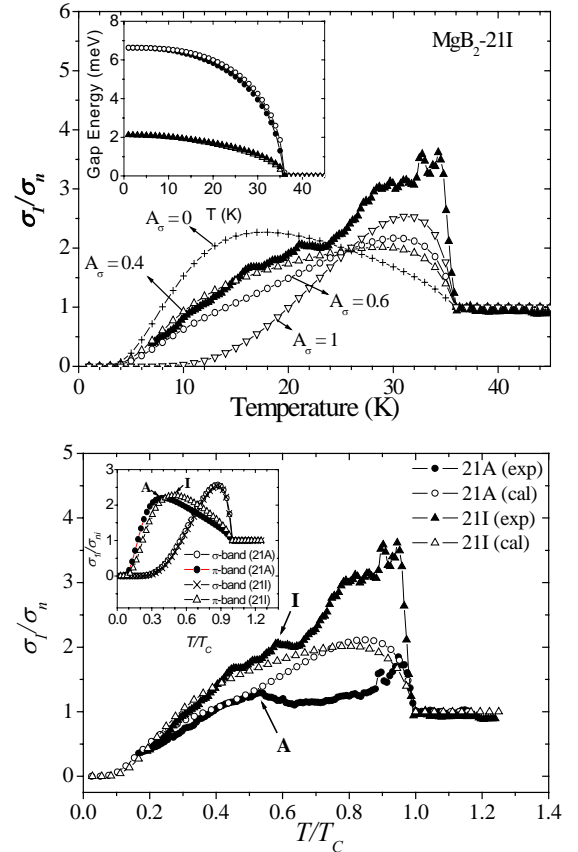


Fig. 4. (a) The measured temperature dependence of σ_1/σ_n for MgB₂-21I compared with the calculated σ_1/σ_n for different values of A_σ and B_π in Eq. (3). The best fitted results are seen for $A_\sigma = 0.4$ and $B_\pi = 0.6$ at temperatures below 25 K. Inset: A comparison between the calculated gap energy values using Eq. (6) (filled symbols) and those using the strong-coupling theory (open symbols) for the σ -band and the π -band of MgB₂-21I. The difference between the values appears smaller than that for MgB₂-21A throughout the measured temperature range. (b) The normalized σ_1 as a function of the reduced temperature T/T_C for MgB₂-21A and MgB₂-21I. Both the measured (filled symbols) values and the fitted ones (open symbols) are shown. The peak in the σ_1/σ_n curve at $T/T_C \sim 0.53$ for MgB₂-21A (labeled 'A') appears shifted to the right with that at $T/T_C \sim 0.61$ for MgB₂-21I (labeled 'I') while no noticeable change is seen for the peak at $T/T_C \sim 0.9$. Inset: The temperature dependence of the normalized σ_{1i} (σ_{1i}/σ_{ni}) for the σ -band ($i = 1$, circle) and the π -band ($i = 2$, triangle) calculated using the coupling constants for MgB₂-21A and those for MgB₂-21I.

between MgB₂-21A and MgB₂-21I might be due to disorders introduced in the MgB₂ film during the ion-milling process and/or attributed to the difference in magnesium stoichiometry and oxygen alloying into the boron layers through the thickness of the MgB₂ film as pointed out by Yates *et al.*²⁷ and Eom *et al.*²⁸ An earlier theoretical work shows that enhanced inter-band scattering in a two-gap model of superconductivity indeed increases the smaller gap value despite the reduction of T_C ²⁹.

The difference in the microwave conductivity data between ours and Jin *et al.*'s¹¹ cannot be clearly understood at the moment. Since the crystal orientation of our polycrystalline samples is different from Jin *et al.*'s having *c*-axis orientations, it is tempting to attribute the observed discrepancy to the difference in the orientations of the MgB₂ grains relative to the direction of the measuring currents, considering the nature of the σ -band having a two-dimensional symmetry. Here it is noted that the microwave conductivity was measured with circulating currents flowing on the surface of the MgB₂ films because only the electric field component E_ϕ is available in both experiments employing the TE₀₁₁ mode resonator method. However, the difference in the crystal orientations doesn't seem to provide the correct reason considering that the direction of the electric field is parallel to the *a*-*b* plane when the TE₀₁₁ mode was used for investigating the properties of *c*-axis-oriented MgB₂ film. In other words, the peak near the T_C due to the σ -band would be better observed from a sample having *c*-axis oriented grains, as has been reported in a theoretical work by Dolgov³⁰, if the scattering rate in the σ -band is not extremely different from that in the π -band. There is also a recent report by Gennaro *et al.* on an experimental observation of the coherence peak near T_C for polycrystalline MgB₂³¹. Further studies are needed to address the correct reasons for this.

We note that, considering the three-dimensional nature of the π -band gap and the strong inter-grain coupling among the grains, the $A_\pi(0)$ values of our films are believed to be reflect the intrinsic properties of our films despite that they are polycrystalline. Since the σ_I values due to the π -band with the smaller energy gap are much larger than those due to the σ -band at low temperatures, this might explain why good agreements were found between the measured and the calculated σ_I at low temperatures below 20 – 25 K (see e.g. Fig. 3(a) and the inset of Fig. 4(b) for the σ_I values solely due to the π -band ($A_\sigma = 0$) and the σ -band ($A_\sigma = 1$)). At temperatures above 20 – 25 K where contribution of the σ -band to σ_I becomes dominant, it seems necessary to take the relative orientation of the MgB₂ grains with respect to the direction of the applied electric field into account in

calculating the σ_I values, considering the two-dimensional nature of the σ -band.

Our results suggest that microwave properties of MgB₂ films with enhanced inter-band scattering could be improved at low temperatures due to the enhanced energy gap in the π -band despite reduction of the T_C due to the suppressed energy gap in the σ -band. We note that enhanced microwave properties have previously been observed in the ion-milled MgB₂ films not only in their linear microwave properties such as the R_S , but also in their nonlinear microwave properties such as the third harmonic intercept as reported by Booth *et al.*³². With the s-wave nature of the order parameters of MgB₂ considered, even a small enhancement of the energy gap in the π -band by controlled introduction of disorders to the material is expected to lead to substantial improvements in the overall microwave properties.

IV. Conclusions

The temperature dependences of the surface resistance and the microwave conductivity were measured for high-quality polycrystalline MgB₂ films at ~8.5 GHz before and after ion-milling. Two coherence peaks were observed at $T/T_C \sim 0.5$ - 0.6 and $T/T_C \sim 0.9$ in the temperature dependence of the microwave conductivity for both films with the peak due to the π -band appearing at different reduced temperatures of $T/T_C \sim 0.53$ for the as-grown film and $T/T_C \sim 0.61$ for the ion-milled film, which is in contrast with an earlier observation of single coherence peak at $T/T_C \sim 0.6$ and dominant role of the π -band in the microwave conductivity of *c*-axis oriented MgB₂ films as reported by Jin *et al.*¹¹. Reduction of T_C by 3 K and reduced normal-state conductivity at T_C were observed along with a reduced R_S at temperatures below ~ 15 K for the ion-milled film. The π -band gap energy of the ion-milled MgB₂ film also appeared significantly enhanced with the value of 2.1 meV compared to 1.8 meV for the as-grown MgB₂ film. The reduced R_S of the ion-milled MgB₂ film appeared attributable to the reduced σ_I . Calculations based on the gap energies from the weak coupling BCS theory suggest that both the σ -band and the π -band contribute to σ_I of the polycrystalline MgB₂ films significantly with similar results obtained using the gap energies from the strong coupling theory. Increased T/T_C at which the coherence peak due to π -band is found as well as reduction of T_C observed for the ion-milled film could be explained by increased inter-band coupling constants between the σ -band and the π -band which is attributable to increased disorder in the ion-milled film.

Our results suggest that enhanced energy gap in the π -band of MgB₂ films due to enhanced inter-band scattering

could lead to improved microwave properties at low temperatures despite reduction of the T_C .

Acknowledgments

The authors would like to thank M. J. Kim for her help in collecting data and K. T. Leong for useful discussions. We also thank Hyoungh Joon Choi, Thomas Dahm and Frank Marsiglio for valuable conversations. The work of S. Y. Lee was partially supported by KOSEF under grant no. R01-2001-00038 and by Korean Ministry of Science and Technology. HJH was supported by Korea Research Foundation Grant (KRF-2002-003-C00042).

-
- [1] J. Nagamatsu *et al.*, Nature (London) 410, 63 (2001).
 [2] A. Y. Liu, I. I. Mazin, and J. Kortus, Phys. Rev. Lett. 87, 087005 (2001).
 [3] H. J. Choi, D. Roundy, H. Sun, M. L. Cohen, and S. G. Louie, Nature, 418, 758 (2002); In obtaining the gap energies from the strong coupling theory, we used the temperature dependence of $\Delta(T) = \Delta(0) \times \{1 - (T/T_C)^p\}^{1/2}$ with $p = 2.9$ for the σ -band and $p = 1.8$ for the π -band, respectively.
 [4] P. Szabo *et al.*, Phys. Rev. Lett. 87, 137005 (2001); F. Giubileo *et al.*, Phys. Rev. Lett. 87, 177008 (2001).
 [5] See e.g., C. Buzea and T. Yamashita, Supercond. Sci. Technol., 14, R115-R146 (2001), and references therein.
 [6] F. Bouquet, R. A. Fisher, N. E. Phillips, D. G. Hinks, and J. D. Jorgensen, Phys. Rev. Lett. 87, 047001 (2001).
 [7] A. A. Golubov, J. Kortus, O. V. Dolgov, O. Jepsen, Y. Kong, O. K. Andersen, B. J. Gibson, K. Ahn and R. K. Kremer, J. Phys.: Condens. Matter 14, 1353 (2002).
 [8] S. L. Bud'ko *et al.* Phys. Rev. B 64, 180506 (2001); M. Angst *et al.* Phys. Rev. Lett. 88, 167004 (2002); L. Lyard *et al.* Phys. Rev. B 66, 180502(R) (2002); U. Welp *et al.* Phys. Rev. B 67, 012505 (2003).
 [9] T. Dahm and N. Schopohl, Phys. Rev. Lett. 91, 017001 (2003).
 [10] M.-S. Kim, J. A. Skinta, T. R. Lemberger, W. N. Kang, H.-J. Kim, E.-M. Choi, and S.-I. Lee, Phys. Rev. B 66, 064511 (2002); We note that Kim *et al.*'s analysis has been performed with an assumption that their MgB₂ films are in the clean limit.
 [11] B. B. Jin, T. Dahm, A. I. Gubin, E.-M. Choi, H. J. Kim, Sung-Ik Lee, W. N. Kang and N. Klein, Phys. Rev. Lett. 91, 127006 (2003).
 [12] J. H. Claassen, M. L. Wilson, J. M. Byers, and S. Adrian, J. Appl. Phys. 82, 3028 (1997).
 [13] S. Y. Lee, J. H. Lee, J. Lim, H. N. Lee, S. H. Moon, B. Oh, and M. Hein, IEEE Trans. Appl. Supercond. 13, 3585 (2003).
 [14] S. H. Moon, J. H. Yun, H. N. Lee, J. I. Kye, H. G. Kim, W. Chung, and B. Oh, Appl. Phys. Lett. 79, 2429 (2001).
 [15] S. Y. Lee, J. H. Lee, Jung H. Lee, J. S. Ryu, and J. Lim, S. H. Moon, H. N. Lee, H. G. Kim, and B. Oh, Appl. Phys. Lett. 79, 3299 (2001), and references therein.
 [16] S. Y. Lee, J. H. Lee, M. J. Kim, V. B. Fedorov, J. C. Booth, K. Leong, S. Schima, D. Rudman (unpublished).
 [17] M. J. Lancaster, Passive Microwave Device Applications of High-Temperature Superconductors, Cambridge, United Kingdom, 1997, Cambridge University Press, ch. 1
 [18] N. Klein, H. Chaloupka, G. Müller, S. Orbach, H. Piel, B. Roas, L. Schultz, U. Klein, and M. Peiniger, J. Appl. Phys. 67, 6940 (1990).
 [19] B. B. Jin, N. Klein, W. N. Kang, H.-J. Kim, E.-M. Choi, S.-I. Lee, T. Dahm and K. Maki, Supercond. Sci. Technol. 16, 205 (2003).
 [20] N. Hakim, C. Kusko, S. Sridhar, A. Soukiassian, X. H. Zeng, and X. X. Xi, Appl. Phys. Lett. 81, 3603 (2002).
 [21] M. A. Hein, M. Getta, S. Kreiskott, B. Moenter, H. Piel, D. E. Oates, P. J. Hirst, R. G. Humphreys, H. N. Lee, and S. H. Moon, Physica C 372-376, 571 (2002).
 [22] I. I. Mazin, O. K. Andersen, O. Jepsen, O. V. Dolgov, J. Kortus, A. A. Golubov, A. B. Kuzmenko, and D. Van der Marel, Phys. Rev. Lett. 89, 107002 (2002).
 [23] D. C. Mattis and J. Bardeen, Phys. Rev. 111, 412 (1958).
 [24] Note that we used the coupling constant of $\lambda_{II} = 0.94$, a value smaller than the value of $\lambda_{II} = 0.98$ by Liu *et al.*², to get the calculated T_C of ~ 39 K. Much smaller coupling constants need to be used to get the similar gap energies if we use $\hbar\omega_C = 56$ meV in Eq. (6) as has been reported by Jin *et al.*¹¹.
 [25] S. V. Barabash and D. Stroud, Phys. Rev. B 66, 172501 (2002).
 [26] A. Brinkman, A. Golubov, H. Rogalla, O. V. Dolgov, J. Kortus, Y. Kong, O. Jepsen, and O. Andersen, Phys. Rev. B 65, 180517(R) (2002).
 [27] K. A. Yates, G. Burnell, N. A. Stelmashenko, D.-J. Kang, H. N. Lee, B. Oh, and M. G. Blamire, cond-mat/03054661 (2003).
 [28] C. Eom, M. Lee, J. Choi, L. Belenky, X. Song, L. Cooley, M. Naus, S. Patnaik, J. Jiang, M. Rikel, *et al.*, Nature (London) 411, 558 (2001).
 [29] N. Schopohl and K. Scharnberg, Solid State Commun. 22, 371 (1977).
 [30] O. V. Dolgov (unpublished).
 [31] E. Di Gennaro, M. Putti, C. Ferdeghini, G. Lamura, and A. Andreone (unpublished).
 [32] J.C. Booth, S. Y. Lee, K. T. Leong, J. H. Lee, J. Lim, H. N. Lee, S. H. Moon, and B. Oh, IEEE Trans. Appl. Supercond. 13, 3590 (2003); .